Progress In Electromagnetics Research, Vol. 137, 669–685, 2013

MODELING SAR IMAGES BASED ON A GENERALIZED GAMMA DISTRIBUTION FOR TEXTURE COMPONENT

Gui Gao*, Xianxiang Qin, and Shilin Zhou

College of Electronic Science and Engineering, National University of Defense Technology, Changsha, Hunan 410073, P. R. China

Abstract—In the applications of synthetic aperture radar (SAR) data, a crucial problem is to develop precise models for the statistics of the pixel amplitudes or intensities. In this paper, a new statistical model, called simply here $G\Gamma\Gamma$, is proposed based on the product model by assuming the radar cross section (RCS) components (texture components) of the return obey a recently empirical generalized Gamma distribution. Meanwhile, we demonstrate theoretically that the proposed $G\Gamma\Gamma$ model has the well-known $\mathcal{K}$ and $\mathcal{G}^{\circ}$ distributions as special cases. We also derived analytically the estimators of the presented $G\Gamma\Gamma$ model by applying the "method-of-log-cumulants" (MoLC). Finally, the performance of the proposed model is tested by using some measured SAR images.

1. INTRODUCTION

There has been growing interest in synthetic aperture radar (SAR) image interpretation for a variety of civilian and military applications [1, 2], such as terrain classification [3–5], land or sea monitoring [6–8], target detection and recognition [9–13], etc. Presently, one of the major strategies of SAR image processing is to use the classical methods of statistical pattern recognition, where it is crucial to develop precise models for the statistics of the pixel amplitudes or intensities [14–17].

Studies on statistical models of SAR images with different terrain types have been carried out over the last couple of decades. In summary, three main solutions, i.e., parametric models [17, 18], non-parametric models [15, 19] and mixture models [20], can be employed

Received 18 January 2013, Accepted 28 February 2013, Scheduled 8 March 2013

* Corresponding author: Gui Gao (dellar@126.com).

for this purpose. Specifically, as a modeling way of the data-driven, non-parametric approaches, e.g., probabilistic neural network (PNN) [15, 21–23] and standard Parzen window estimator [19, 24], have proved to be effective estimated tools and suitable for estimating the complex or unknown probability density function (PDF). However, as vast computational load and numerous data involved, non-parametric approaches are limited in the various applications. Consequently, parametric models turn out to be intensively investigated in many literatures [14, 15, 17, 18]. The process of parametric modeling can be described in brief as to choose the appropriate one from several analytical statistical distributions for the given image. Practically, it is not sufficient for fitting a large-scale scene by parametric models due to the complex contexts and numerous terrain types included [15]. The mixture models, combining two or more parametric models, provide a creative idea for this problem. Several alternatives, such as Gamma mixture model [20], the finite mixture models [25], etc., are given. Unfortunately, the estimates of parameters are a hard task for this kind of models. Similarly with the time-consuming of non-parametric approaches, a common strategy, for instance, using expectation-maximization (EM) algorithm [20, 25], often tends to be tediously iterative.

Focusing on parametric models, the product model [15, 17], expressed as the product of an underlying radar cross section (RCS) [26–28] with an uncorrelated multiplicative speckle noise one, has been widely and successfully used in conducting the analytical mathematic formulas to describe the statistical properties of SAR data. Some studies have been presented based on this model in the past several decades, such as Γ [15], $\mathcal{K}$ [17] etc.. Among these distributions, an important contribution is the derivation of the famous $\mathcal{G}^{\circ}$ distribution by Frery [14], under the consideration of discriminating types of homogeneous, heterogeneous and extremely heterogeneous terrains. This distribution encompasses most of the existing models, mainly because the reciprocal of a Gamma (also called the inverse Gamma) distribution [14, 15] can match the RCS components of different terrain types. Recently, Li et al. [29] proposed an empirical generalized Gamma distribution ($G\Gamma D$) to estimate the PDFs of SAR data. Although this distribution is a purely mathematical model and has no relation to the physics of wave scattering [26–28], many well-known distributions, such as Rayleigh, exponential, Nakagami, Gamma, Weibull, log-normal and inverse Gamma distributions, are particular cases of this $G\Gamma D$ [29].

Motivated by aforementioned characteristic, this paper is devoted to develop a novel statistical model (denoted simply as $G\Gamma\Gamma$) to model

different types of clutter with respect to pixel amplitude or intensity in high-resolution SAR images. The proposed model arises using $G\Gamma D$ proposed to describe the RCS components of amplitude or intensity return based on the product model. As discussed in Section 2, it could be proven theoretically that the new model has the $\mathcal{K}$ distribution for heterogeneous clutter as well as the $\mathcal{G}^{\circ}$ distribution for extremely heterogeneous clutter as special cases. Furthermore, using the second-kind statistics theory developed by Nicolas [30], which relies on the Mellin transform, i.e., "method-of-log-cumulants" (MoLC), we derive the parameter estimators of the new distribution model.

The present paper has been divided as follows. In Section 2, a derivation of the proposed $G\Gamma\Gamma$ model is given. In Section 3, the parametric estimator of the presented statistical model is also derived analytically based on the Mellin transform. We provide the experimental results of the $G\Gamma\Gamma$ model using typical measured SAR data in Section 4. The last section concludes this paper.

2. THE PROPOSED $G\Gamma\Gamma$ MODEL

2.1. The $G\Gamma D$ and the Product Models

The generalized gamma distribution is recently defined as [29]

$$p_X(x) = \frac{|v|\,\kappa^{\kappa}}{\sigma\Gamma(\kappa)}\left(\frac{x}{\sigma}\right)^{\kappa v-1}\exp\left\{-\kappa\left(\frac{x}{\sigma}\right)^{v}\right\},\quad \sigma,|v|,\kappa,x>0 \tag{1}$$

where v, κ and σ are the power, shape and scale parameters, respectively. $\Gamma(\cdot)$ represents the Gamma function. The PDF characterized by (1) is shown as an empirical model. It is an ideal alternative for modeling the RCS components of SAR intensity or amplitude return, owing to that both the Gamma distribution (describing the heterogeneous clutter) and the inverse Gamma one (describing the extremely heterogeneous terrains) can be viewed as particular cases of this general model [29], and correspond to $v = 1$ and $v = -1$, respectively.

The product model [15, 17] has been testified that it is valid for conducting statistical models of amplitude or intensity statistics of SAR data. Its expression is given by

$$Z = X \cdot Y \tag{2}$$

where X and Y indicate the backscattering RCS component and speckle noise one, respectively, Z denotes the observed intensity or amplitude of SAR data. To make a clear distinction, a similar strategy with literature [14], i.e., the subscripts "I" and "A", will be used separately hereafter for the intensity and amplitude cases. Considering

the case of the intensity, it is widely accepted that multilook intensity speckle noise component obeys the Gamma distribution [15, 17] with unitary mean, whose PDF is expressed by

$$p_{Y_I}(y) = \frac{n^n}{\Gamma(n)} y^{n-1} \exp(-ny), \quad y, n > 0 \tag{3}$$

where n is the number of looks.

2.2. The $G\Gamma\Gamma$ Model

Herein, within the structure of the product model shown in (2), combining (3) and (1), the PDF of Z_I can be derived as

$$p_{Z_I}(z) = \int_0^\infty \frac{1}{x} \cdot p_{X_I}(x) \cdot p_{Y_I}\left(\frac{z}{x}\right) dx = \frac{|v|\,\kappa^\kappa n^n}{\sigma^{\kappa v}\Gamma(\kappa)\Gamma(n)} z^{n-1} \int_0^\infty x^{\kappa v - n - 1} \exp\left\{-\kappa\left(\frac{x}{\sigma}\right)^v - n\left(\frac{z}{x}\right)\right\} dx, \quad \sigma, \kappa, n, z > 0,\ v \neq 0 \tag{4}$$

Its moments [31–33] of m order turn out to be (see Appendix A):

$$E(z_I^m) = \frac{\Gamma(m+n)}{\Gamma(\kappa)\Gamma(n)} \Gamma\left(\kappa + \frac{m}{v}\right) \left(\frac{\sigma \kappa^{-1/v}}{n}\right)^m \tag{5}$$

In order to facilitate the numerical integral in (4), a transform, $x = \tan(\theta)$, leads to that (4) could be rewritten as

$$p_{Z_I}(z) = \frac{|v|\,\kappa^\kappa n^n}{\sigma^{\kappa v}\Gamma(\kappa)\Gamma(n)} z^{n-1} \cdot \int_0^{\frac{\pi}{2}} \sec^2(\theta) \tan^{\kappa v - n - 1}(\theta) \exp\left\{-\kappa\left(\frac{\tan(\theta)}{\sigma}\right)^v - n\left(\frac{z}{\tan(\theta)}\right)\right\} d\theta, \quad \sigma, \kappa, n, z > 0,\ v \neq 0 \tag{6}$$

Letting Z_A denote the amplitude return, via the relationship of $p_{Z_A}(z) = 2z p_{Z_I}(z^2)$, and thus the PDF of Z_A is characterized by

$$p_{Z_A}(z) = \frac{2\,|v|\,\kappa^\kappa n^n}{\sigma^{\kappa v}\Gamma(\kappa)\Gamma(n)} z^{2n-1} \cdot \int_0^{\frac{\pi}{2}} \sec^2(\theta) \tan^{\kappa v - n - 1}(\theta) \exp\left\{-\kappa\left(\frac{\tan(\theta)}{\sigma}\right)^v - n\left(\frac{z^2}{\tan(\theta)}\right)\right\} d\theta, \quad \sigma, \kappa, n, z > 0,\ v \neq 0 \tag{7}$$

We refer to this distribution characterized by (6) or (7) as the generalized Gamma Gamma distribution, abbreviated as $G\Gamma\Gamma$ distribution. Specifically, we call the $G\Gamma\Gamma_I$ distribution and the $G\Gamma\Gamma_A$ distribution, correspond to (6) and (7), respectively, to distinct the intensity statistic as well as the amplitude statistic. Figure 1 gives the plots of the $G\Gamma\Gamma_A$ distribution with respect to the various parameters.

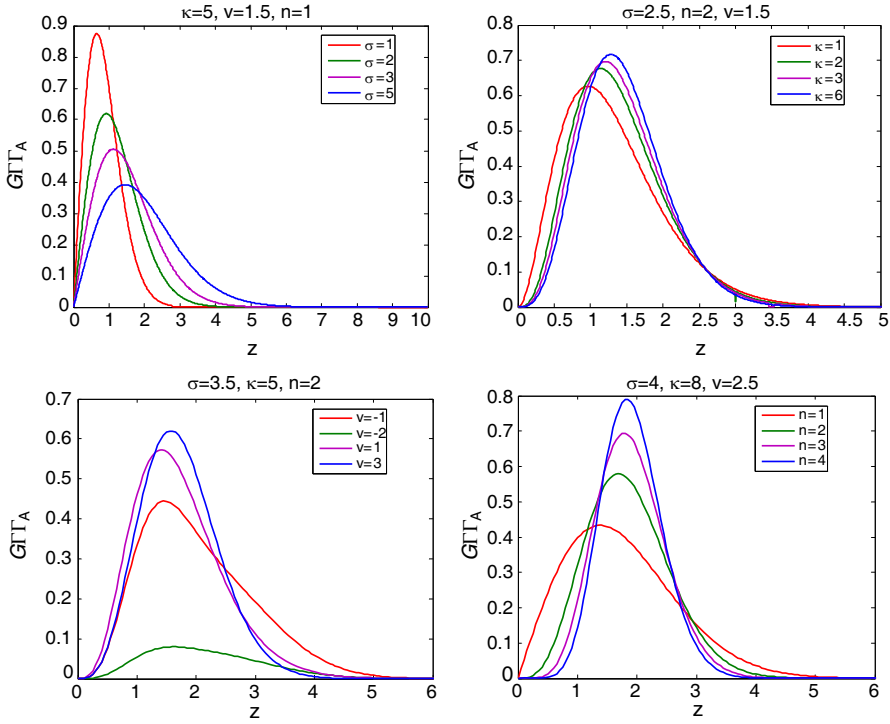

Figure 1. Plots of $G\Gamma\Gamma_A$ vs. different parameters.

Additionally, it can be proven (see Appendix B) theoretically that the $G\Gamma\Gamma$ is degenerating to the well-known $\mathcal{G}^\circ$ and $\mathcal{K}$ on the conditions of $v = -1$ and $v = 1$, respectively. This property stated means that the proposed $G\Gamma\Gamma$ distribution encompasses the modeling abilities of $\mathcal{G}^\circ$ and $\mathcal{K}$ whilst extending them to enable the modeling of the clutter areas with more widely varying degrees of homogeneity.

3. PARAMETER ESTIMATOR OF THE $G\Gamma\Gamma$ MODEL BASED ON MOLC

3.1. The Log-Cumulants of $G\Gamma\Gamma$

The MoLC [18, 30] has been proposed by Nicolas et al. as a parametric PDF estimation technique for a function defined over $\mathbb{R}^+$. MoLC is based on a second kind statistics by applying the Mellin transform, instead of the Fourier and Laplace transforms. Given a positive-valued random variable X with the PDF $p_X(x)$, the second-kind first

characteristic function is defined as the Mellin transform of $p_X(x)$:

$$\phi_X(s) = \mathcal{M}[p_X(x)](s) = \int_0^\infty x^{s-1} p_X(x) dx \tag{8}$$

where $\mathcal{M}$ is the Mellin transform operator. Subsequently, the second characteristic function of the second kind is computed as the natural logarithm of $\phi_X(s)$:

$$\varphi_X(s) = \log(\phi_X(s)) \tag{9}$$

The r-th order derivative of $\varphi_X(s)$ at $s = 1$ is the second kind cumulants (also named log-cumulants) of order r, i.e.,

$$\tilde{c}_r = \left. \frac{d^r \varphi_X(s)}{ds^r} \right|_{s=1} \tag{10}$$

Thanks to the relation between the Mellin transform and the moments of random variable, i.e., $\phi_X(s) = E\left(X^{s-1}\right)$. Hence, via (5), the second-kind first and second characteristic functions of the $G\Gamma\Gamma$ distribution are given, respectively, by the following equations:

$$\begin{cases} \phi_{G\Gamma\Gamma}(s) = \frac{\Gamma(s-1+n)}{\Gamma(\kappa)\Gamma(n)} \Gamma\left(\kappa + \frac{s-1}{v}\right) \left(\frac{\sigma}{n\kappa^{\frac{1}{v}}}\right)^{s-1} \\ \varphi_{G\Gamma\Gamma}(s) = \log(\Gamma(s-1+n)) + \log\left(\Gamma\left(\kappa + \frac{s-1}{v}\right)\right) \\ \quad -\log(\Gamma(\kappa)) - \log(\Gamma(n)) + (s-1)(\log(\sigma) - \log(n) - \frac{1}{v}\log(\kappa)) \end{cases} \tag{11}$$

From (10) and (11), one can obtain the log-cumulants of the $G\Gamma\Gamma$ distribution expressed by

$$\begin{cases} \tilde{c}_1 = \Psi(n) + \log(\sigma/n) + (\Psi(\kappa) - \log(\kappa))/v \\ \tilde{c}_r = \Psi(r-1, n) + \Psi(r-1, \kappa)/v^r, \; r \geq 2 \end{cases} \tag{12}$$

where $\Psi(\cdot)$ represents the digamma function (i.e., the logarithmic derivative of the Gamma function), and $\Psi(r, \cdot)$ is the r-th order Polygamma function (i.e., the rth order derivative of the digamma function).

Given a sample set $\{z_i\}$, $i \in [1, N]$, the estimates of the first three log-cumulants can be acquired directly by

$$\begin{cases} \hat{\tilde{c}}_1 = \frac{1}{N} \sum_{i=1}^{N} [\ln(z_i)] \\ \hat{\tilde{c}}_r = \frac{1}{N} \sum_{i=1}^{N} \left[\left(\ln(z_i) - \hat{\tilde{c}}_1 \right)^r \right], \; r = 2, 3 \end{cases} \tag{13}$$

3.2. The Estimates of Parameters in $G\Gamma\Gamma$

Paying attention to (12), we stress that $\tilde{c}_r,\ r \geq 2$ do not contain σ, thus allowing us to divide the parameter estimates of the $G\Gamma\Gamma$ distribution into three distinct stages.

First, based on (12), the 2-th and 3-th order log-cumulants of the $G\Gamma\Gamma$ distribution yield

$$\tilde{c}_2 = \Psi(1,n) + \Psi(1,\kappa)/v^2 \tag{14}$$

$$\tilde{c}_3 = \Psi(2,n) + \Psi(2,\kappa)/v^3 \tag{15}$$

To isolate v in previous two equations, we take the ratio of $\Psi^3(1,\kappa)/\Psi^2(2,\kappa)$, and thus via (14) and (15), one arrive at that the estimate $\hat{\kappa}$ of the parameter κ is given by

$$\frac{\Psi^3(1,\hat{\kappa})}{\Psi^2(2,\hat{\kappa})} = \frac{\left(\hat{\tilde{c}}_2 - \Psi(1,n)\right)^3}{\left(\hat{\tilde{c}}_3 - \Psi(2,n)\right)^2} \tag{16}$$

As shown in Figure 2, the function on the left-hand-side of (16), $g(\hat{\kappa}) = \Psi^3(1,\hat{\kappa})/\Psi^2(2,\hat{\kappa})$, is strictly monotonically increasing based on the following proof, i.e., the derivation of the function $g(\hat{\kappa})$ vs. the parameter $\hat{\kappa}$ is

$$g'(\hat{\kappa}) = \frac{d}{d\hat{\kappa}}\left[\frac{\Psi^3(1,\hat{\kappa})}{\Psi^2(2,\hat{\kappa})}\right] = \frac{\Psi^2(1,\hat{\kappa})}{\Psi^3(2,\hat{\kappa})}\left[3\Psi^2(2,\hat{\kappa}) - 2\Psi(3,\hat{\kappa})\Psi(1,\hat{\kappa})\right] \tag{17}$$

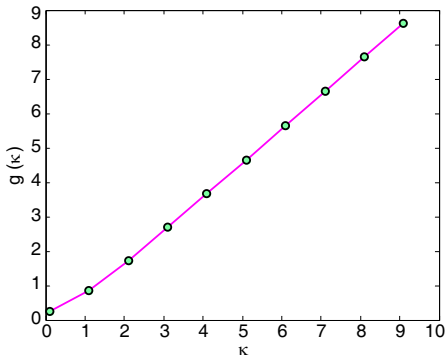

Figure 2. Plot of the function $g(\hat{\kappa})$.

Via [34], the Polygamma function is with the following characteristic:

$$\frac{m-1}{m} < \frac{\Psi^2(m,\hat{\kappa})}{\Psi(m+1,\hat{\kappa})\Psi(m-1,\hat{\kappa})} < \frac{m}{m+1}, \quad \forall \hat{\kappa} > 0,\ m = 2,3,\ldots \tag{18}$$

(18) leads to

$$\frac{1}{2} < \frac{\Psi^2(2,\hat{\kappa})}{\Psi(3,\hat{\kappa})\Psi(1,\hat{\kappa})} < \frac{2}{3} \Rightarrow 3\Psi^2(2,\hat{\kappa}) - 2\Psi(3,\hat{\kappa})\Psi(1,\hat{\kappa}) < 0 \quad (19)$$

Because $\Psi(2,\hat{\kappa}) < 0$ for all $\hat{\kappa} > 0$, it can be observed to conclude that $g'(\hat{\kappa}) > 0$ by taking (19) into (17). A simple numerical solution, for instance, the fsolve function in Matlab or the bisection method [20], can be adopted to obtain the value of $\hat{\kappa}$.

Next, taking $\hat{\kappa}$ into (15) leads to that the estimate $\hat{v}$ of the parameter v is

$$\hat{v} = \sqrt[3]{\frac{\Psi(2,\hat{\kappa})}{\hat{\hat{c}}_3 - \Psi(2,n)}} \quad (20)$$

Finally, plugging $\hat{v}$ and $\hat{\kappa}$ into the first equation of (12), the estimate $\hat{\sigma}$ turns out to be solved.

4. EXPERIMENTAL RESULTS

The aim of this section is to verify the modeling capability of the proposed $G\Gamma\Gamma$ distribution based on the measured SAR data. As discussed in earlier works [14, 15, 18], we note that $\mathcal{G}^\circ$ is an accurate model for SAR images over homogeneous, heterogeneous and extremely heterogeneous terrains (like urban areas), and some conclusions [14, 15, 18] have been made that the $\mathcal{G}^\circ$ distribution outperforms other conventional distributions, such as $\mathcal{K}$, Weibull, Nakagami, etc., in estimating PDFs of given SAR images. On the other hand, by previous analysis, the proposed $G\Gamma\Gamma$ distribution encompasses theoretically the modeling abilities of $\mathcal{G}^\circ$ as proven in Appendix B. Hence, we only compare the proposed $G\Gamma\Gamma$ distribution with the $\mathcal{G}^{\circ\dagger}$ one in this section.

It should be emphasized that we have tested the $G\Gamma\Gamma$ and $\mathcal{G}^\circ$ models on various SAR images (e.g., L-band airborne SAR data acquired by the NASA/JPL AIRSAR sensor, SAR data provided by RADARSAT-2 space-borne SAR system operated in C band, TerraSAR-X SAR data of X band and other data provided by Chinese airborne sensors), which involve different bands, platforms, polarimetric modes and spatial resolutions. Consequently, we found that the performances of $G\Gamma\Gamma$ are almost in agreement with that of $\mathcal{G}^\circ$ when fitting the observed histograms of given SAR images in

† Throughout this paper, the estimates of parameters of the $\mathcal{G}^\circ$ distribution adopt the MoLC, the detailed description is given by Tison, et al. [18].

low-resolution and the homogeneous, heterogeneous regions in high-resolution. In other words, these tested results show that the $G\Gamma\Gamma$ distribution can model all cases the $\mathcal{G}^{\circ}$ distribution can, as expected.

Therefore, to better compare the aforementioned two statistical models, we further check them on extremely heterogeneous terrains of high-resolution images. As an example, a large TerraSAR-X spotlight-mode 300 MHz geocoded scene over Beijing of China, acquired on January 31, 2008 at 10:03 UTC, with high-resolution 2 m $\times$ 2.3 m (azimuth $\times$ range) and HH-polarization is used in this paper as shown in Figure 3. Like other cities in the world, Beijing is known for its well-planned urban expansion. Thus, it remains valid for other cities with similar appearance, although hereafter the tested results on Beijing only are given.

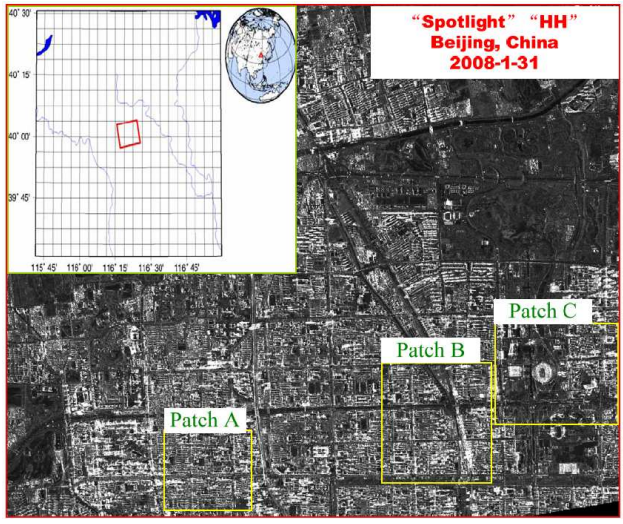

Figure 3. The SAR image of Beijing from the TerraSAR-X.

Three representative patches of extremely heterogeneous areas dominated by urban of buildings and indicated by boxes in Figure 3, numbered A-C (with the sizes of 1476 $\times$ 1342, 1868 $\times$ 1848, and 2361$\times$1720 pixels, respectively), are selected as the main regions of this study. Figures 4–6 show the comparison of the amplitude histograms of the three selected areas indicated in Figure 3 with the proposed $G\Gamma\Gamma$ and classical $\mathcal{G}^{\circ}$ model fits. The estimating results on the linear and logarithmic scales are all provided so that the performance difference in fitting the whole and the tails can be seen clearly.

Before the estimates of other parameters in the proposed $G\Gamma\Gamma$

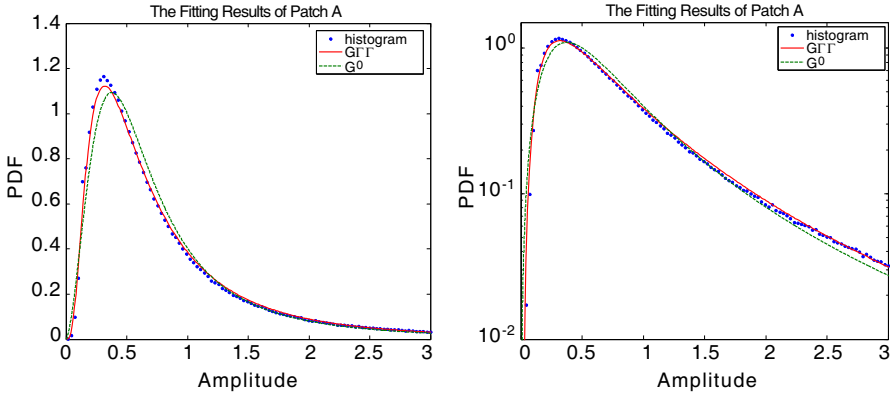

Figure 4. Plots of amplitude histogram for Patch A and of the estimated $G\Gamma\Gamma$ and $\mathcal{G}^{\circ}$ PDFs ((a) in linear scale, (b) in logarithmic scale).

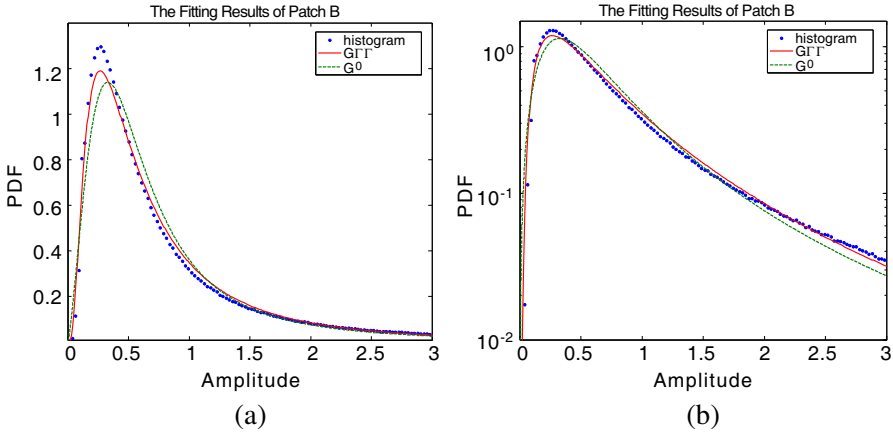

Figure 5. Plots of amplitude histogram for Patch B and of the estimated $G\Gamma\Gamma$ and $\mathcal{G}^{\circ}$ PDFs ((a) in linear scale, (b) in logarithmic scale).

distribution characterized by (6) or (7), the number of looks n is replaced by the ENL. Thus, the estimate $\hat{n}$ of n is equal to 2.22 about the scene as shown in Figure 3 by using homogeneous areas. Next, the parameter estimations of each distribution in Figures 4–6 are all accomplished by the estimators based on the MoLC, which are shown at Table 1, where the analytical expression of the $\mathcal{G}^{\circ}$ distribution is given in (B1).

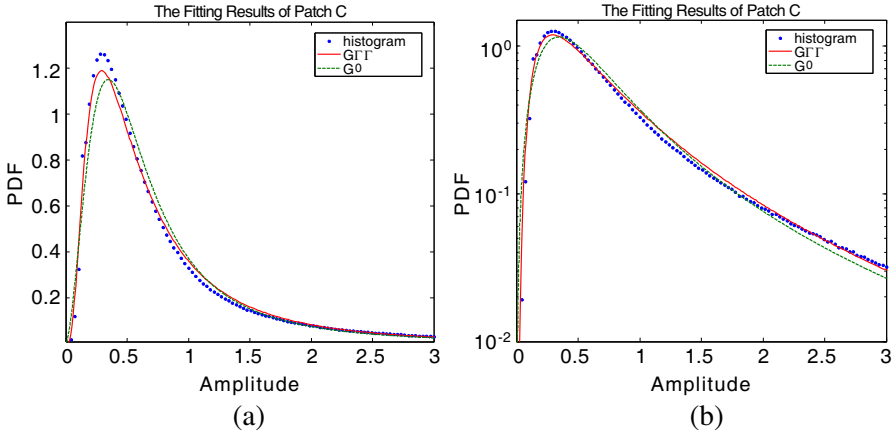

Figure 6. Plots of amplitude histogram for Patch C and of the estimated $G\Gamma\Gamma$ and $\mathcal{G}^{\circ}$ PDFs ((a) in linear scale, (b) in logarithmic scale).

Table 1. Parameter estimations of noted areas in Figure 3.

Patches	$G\Gamma\Gamma$ $(\hat{\sigma}, \hat{\kappa}, \hat{v})$	$\mathcal{G}^{\circ}$ $(\hat{\alpha}, \hat{\gamma}, \hat{n})$
A	(0.3781, 4.0953, −0.3360)	(−0.9260, 0.3332, 1.2713)
B	(0.3229, 4.3008, −0.2990)	(−0.8379, 0.2584, 1.1484)
C	(0.3239, 3.1509, −0.3744)	(−0.8630, 0.2708, 1.2668)

In order to quantitatively assess the fitting result, we adopt the Kolmogorov-Smirnov (KS) test [15] as a similarity measurement. The smaller the value of KS measurement obtains, the higher fitting accuracy they have. The KS values of the fitting results shown in Figures 4–6 are compared in Table 2. From this table, it can be conclude that the proposed $G\Gamma\Gamma$ distribution well agrees with the given SAR images, which implies the higher precision of fitting using $G\Gamma\Gamma$ distribution than using $\mathcal{G}^{\circ}$ distribution.

Table 2. The comparison of fitting histogram.

Patches	KS values of $G\Gamma\Gamma$	KS values of $\mathcal{G}^{\circ}$
A	0.0053	0.0131
B	0.0101	0.0206
C	0.0082	0.0153

5. CONCLUSION

In this paper, we have developed a new statistical model, namely $G\Gamma\Gamma$, for SAR image modeling and analysis within the product model by assuming the radar cross section (RCS) components of the return obey an empirical generalized Gamma distribution. We also demonstrate theoretically that the proposed model has the well-known $\mathcal{K}$ and $\mathcal{G}^{\circ}$ distributions as special cases. Additionally, the parameter estimators of the presented model are obtained by applying the MoLC. The experimental results show that this model provides better performance compared to $\mathcal{G}^{\circ}$ distribution, especially in the extremely heterogeneous high-resolution urban areas.

Unfortunately, the proposed model as shown in (6) or (7) is an integral representation, which may bring some limits in practice. Our future works will focus on validating this proposed model in an image processing application such as classification, filtering, detection, etc..

ACKNOWLEDGMENT

The authors would like to thank all the reviewers for their valuable suggestions and comments. This paper is supported by the National Natural Science Foundation of China (No. 41171316).

APPENDIX A. THE DERIVATION OF m-th ORDER MOMENTS OF THE $G\Gamma\Gamma$ DISTRIBUTION

Via (4), The m-th order moment estimation of $G\Gamma\Gamma$ is

$$\begin{aligned} E\left(z_I^m\right) &= \int_0^\infty z^m f_{Z_I}(z)dz = \int_0^\infty z^m \frac{|v|\,\kappa^\kappa n^n}{\sigma^{\kappa v}\Gamma(\kappa)\Gamma(n)} z^{n-1} \\ &\quad \int_0^\infty x^{\kappa v-n-1} \exp\left\{-\kappa\left(\frac{x}{\sigma}\right)^v - n\left(\frac{z}{x}\right)\right\} dxdz \\ &= \frac{|v|\,\kappa^\kappa n^n}{\sigma^{\kappa v}\Gamma(\kappa)\Gamma(n)} \int_0^\infty x^{\kappa v-n-1} \exp\left\{-\kappa\left(\frac{x}{\sigma}\right)^v\right\} \\ &\quad \int_0^\infty z^{m+n-1} \exp\left\{-n\left(\frac{z}{x}\right)\right\} dzdx \end{aligned} \tag{A1}$$

Letting $t = nz/x$, then $z = tz/x$ and $dz = \frac{x}{n}dt$. Due to $z : 0 \to \infty$,

$t:0\to\infty$. Thus, the integral of right-hand side in (A1) is given by

$$\int_0^\infty z^{m+n-1}\exp\left\{-n\left(\frac{z}{x}\right)\right\}dz=\int_0^\infty\left(\frac{tx}{n}\right)^{m+n-1}\exp\{-t\}\frac{x}{n}dt$$
$$=\left(\frac{x}{n}\right)^{m+n}\int_0^\infty t^{m+n-1}\exp\{-t\}\,dt=\left(\frac{x}{n}\right)^{m+n}\Gamma(m+n) \tag{A2}$$

Taking (A2) into (A1), (A1) can be simplified as

$$E\left(z_I^m\right)=\frac{|v|\kappa^\kappa n^n}{\sigma^{\kappa v}\Gamma(\kappa)\Gamma(n)}\int_0^\infty x^{\kappa v-n-1}\exp\left\{-\kappa\left(\frac{x}{\sigma}\right)^v\right\}\left(\frac{x}{n}\right)^{m+n}\Gamma(m+n)dx$$
$$=\frac{|v|\,\kappa^\kappa\Gamma(m+n)}{\sigma^{\kappa v}\Gamma(\kappa)\Gamma(n)n^m}\int_0^\infty x^{\kappa v+m-1}\exp\left\{-\kappa\left(\frac{x}{\sigma}\right)^v\right\}dx \tag{A3}$$

A change of $t=\kappa\left(\frac{x}{\sigma}\right)^v$ leads to $x=\sigma\left(\frac{t}{\kappa}\right)^{1/v}$ and $dx=\frac{\sigma}{\kappa v}\left(\frac{t}{\kappa}\right)^{1/v-1}dt$, where $x:0\to\infty$, then $t:\begin{cases}0\to\infty, & v>0\\ \infty\to 0, & v<0\end{cases}$. Thus, two cases are divided. When $v>0$, we obtain

$$E\left(z_I^m\right)$$
$$=\frac{|v|\,\kappa^\kappa\Gamma(m+n)}{\sigma^{\kappa v}\Gamma(\kappa)\Gamma(n)n^m}\int_0^\infty\sigma^{\kappa v+m-1}\left(\frac{t}{\kappa}\right)^{\frac{\kappa v+m-1}{v}}\exp\{-t\}\frac{\sigma}{\kappa v}\left(\frac{t}{\kappa}\right)^{1/v-1}dt$$
$$=\frac{v\Gamma(m+n)\sigma^m}{v\Gamma(\kappa)\Gamma(n)n^m\kappa^{\frac{m}{v}}}\int_0^\infty t^{\kappa+\frac{m}{v}-1}\exp\{-t\}\,dt$$
$$=\frac{\Gamma(m+n)}{\Gamma(\kappa)\Gamma(n)}\Gamma\left(\kappa+\frac{m}{v}\right)\left(\frac{\sigma\kappa^{-1/v}}{n}\right)^m \tag{A4}$$

Oppositely, if $v<0$, (A3) is expressed by

$$E\left(z_I^m\right)$$
$$=\frac{|v|\,\kappa^\kappa\Gamma(m+n)}{\sigma^{\kappa v}\Gamma(\kappa)\Gamma(n)n^m}\int_\infty^\circ\sigma^{\kappa v+m-1}\left(\frac{t}{\kappa}\right)^{\frac{\kappa v+m-1}{v}}\exp\{-t\}\frac{\sigma}{\kappa v}\left(\frac{t}{\kappa}\right)^{1/v-1}dt$$
$$=\frac{-v\Gamma(m+n)\sigma^m}{v\Gamma(\kappa)\Gamma(n)n^m\kappa^{\frac{m}{v}}}\int_\infty^\circ t^{\kappa+\frac{m}{v}-1}\exp\{-t\}\,dt$$
$$=\frac{v\Gamma(m+n)\sigma^m}{v\Gamma(\kappa)\Gamma(n)n^m\kappa^{\frac{m}{v}}}\int_0^\infty t^{\kappa+\frac{m}{v}-1}\exp\{-t\}\,dt$$
$$=\frac{\Gamma(m+n)}{\Gamma(\kappa)\Gamma(n)}\Gamma\left(\kappa+\frac{m}{v}\right)\left(\frac{\sigma\kappa^{-1/v}}{n}\right)^m \tag{A5}$$

(A4) or (A5) are completely identical to the expression shown in (5).

APPENDIX B. PROOF OF THE RELATIONSHIP BETWEEN DISTRIBUTIONS

B.1. Proof of $G\Gamma\Gamma \overset{v=-1}{\rightarrow} \mathcal{G}^{\circ}$

On the condition of $v=-1$, (4) turns out to be

$$f_{Z_I}(z)=\frac{\kappa^{\kappa}n^n}{\sigma^{-\kappa}\Gamma(\kappa)\Gamma(n)}z^{n-1}\int_0^{\infty}x^{-\kappa-n-1}\exp\left\{-\kappa\frac{\sigma}{x}-n\left(\frac{z}{x}\right)\right\}dx \quad \text{(B1)}$$

According to the integral formula $\int_0^{\infty}x^{a-1}\exp\{-bx\}\,dx=\frac{1}{b^a}\Gamma(a)$, $\operatorname{Re}a>0,\ \operatorname{Re}b>0$ [34] and making a variable change of $t=1/x$, we yield

$$\begin{aligned}f_{Z_I}(z)&=\frac{\kappa^{\kappa}n^n}{\sigma^{-\kappa}\Gamma(\kappa)\Gamma(n)}z^{n-1}\int_{\infty}^{\circ}-t^{-2}\cdot t^{\kappa+n+1}\exp\{-(\kappa\sigma+nz)t\}\,dt\\&=\frac{\kappa^{\kappa}n^n}{\sigma^{-\kappa}\Gamma(\kappa)\Gamma(n)}z^{n-1}\int_0^{\infty}t^{\kappa+n-1}\exp\{-(\kappa\sigma+nz)t\}\,dt\\&=\frac{\kappa^{\kappa}n^n}{\sigma^{-\kappa}\Gamma(\kappa)\Gamma(n)}z^{n-1}\frac{1}{(\kappa\sigma+nz)^{\kappa+n}}\Gamma(\kappa+n)\end{aligned} \quad \text{(B2)}$$

Letting $\kappa=-\alpha$ and $\gamma=\kappa\sigma$, the well-known intensity $\mathcal{G}^{\circ}$ distribution [14] is obtained, i.e.,

$$f_{Z_I}(z)=\frac{n^n\Gamma(n-\alpha)z^{n-1}}{\gamma^{\alpha}\Gamma(n)\Gamma(-\alpha)(\gamma+nz)^{n-\alpha}},\quad -\alpha,\ \gamma,\ n,\ z>0 \quad \text{(B3)}$$

B.2. Proof of $G\Gamma\Gamma \overset{v=1}{\rightarrow} \mathcal{K}$

Similarly, when $v=1$, (4) can be rewritten as

$$f_{Z_I}(z)=\frac{\kappa^{\kappa}n^n}{\sigma^{\kappa}\Gamma(\kappa)\Gamma(n)}z^{n-1}\int_0^{\infty}x^{\kappa-n-1}\exp\left\{-\kappa\frac{x}{\sigma}-n\left(\frac{z}{x}\right)\right\}dx \quad \text{(B4)}$$

Utilizing the integral formula $\int_0^{\infty}x^{a-1}\exp\left(-\frac{c}{x}-bx\right)dx = 2\left(\frac{c}{b}\right)^{a/2}K_a\left(2\sqrt{cb}\right)$, $\operatorname{Re}b>0,\ \operatorname{Re}c>0$ [34], we further obtain

$$f_{Z_I}(z)=\frac{\kappa^{\kappa}n^n}{\sigma^{\kappa}\Gamma(\kappa)\Gamma(n)}z^{n-1}2\left(\frac{nz\sigma}{\kappa}\right)^{\frac{\kappa-n}{2}}K_{\kappa-n}\left(2\sqrt{nz\kappa/\sigma}\right) \quad \text{(B5)}$$

By the replacement of variable, i.e., $\lambda=\kappa/\sigma$ and $\alpha=\kappa$, we arrive at the $\mathcal{K}$ distribution [14]:

$$f_{Z_I}(z)=\frac{2\lambda n}{\Gamma(\alpha)\Gamma(n)}(\lambda nz)^{\frac{\alpha+n}{2}-1}K_{\alpha-n}\left(2\sqrt{n\lambda z}\right)\quad \alpha,\ \lambda,\ n,\ z>0 \quad \text{(B6)}$$

where $K_{\alpha-n}(\cdot)$ is the second type modified Bessel function with order $\alpha-n$.

REFERENCES

1. Chan, Y. K. and V. C. Koo, "An introduction to synthetic aperture radar (SAR)," *Progress In Electromagnetics Research B*, Vol. 2, 27–60, 2008.
2. Feng, L., H. P. Xu, C. S. Li, S. Li, and H. Gao, "A novel estimation approach of dynamic and coupling baseline for distributed satellite SAR," *Progress In Electromagnetics Research*, Vol. 123, 467–484, 2012.
3. Dusséaux, R., E. Vannier, O. Taconet, and G. Granet, "Study of backscatter signature for seedbed surface evolution under rainfall-influence of radar precision," *Progress In Electromagnetics Research*, Vol. 125, 415–437, 2012.
4. Koo, V. C., Y. K. Chan, V. Gobi, M. Y. Chua, C. H. Lim, C. S. Lim, C. C. Thum, T. S. Lim, Z. Bin Ahmad, K. A. Mahmood, M. H. Bin Shahid, C. Y. Ang, W. Q. Tan, P. N. Tan, K. S. Yee, W. G. Cheaw, H. S. Boey, A. L. Choo, and B. C. Sew, "A new unmanned aerial vehicle synthetic aperture radar for environmental monitoring," *Progress In Electromagnetics Research*, Vol. 122, 245–268, 2012.
5. Du, Y., Y. L. Luo, W. Z. Yan, and J. A. Kong, "An electromagnetic scattering model for soybean canopy," *Progress In Electromagnetics Research*, Vol. 79, 209–223, 2008.
6. Zhao, Y. W., M. Zhang, X. P. Geng, and P. Zhou, "A comprehensive facet model for bistatic SAR imagery of dynamic ocean scene," *Progress In Electromagnetics Research*, Vol. 123, 427–445, 2012.
7. Albert, M. D., Y. J. Lee, H. T. Ewe, and H. T. Chuah, "Multilayer model formulation and analysis of radar backscattering from sea ice," *Progress In Electromagnetics Research*, Vol. 128, 267–290, 2012.
8. Bausssard, A., M. Rochdi, and A. Khenchaf, "Po/mec-based scattering model for complex objects on a sea surface," *Progress In Electromagnetics Research*, Vol. 111, 229–251, 2011.
9. Mohammadpoor, M., R. S. A. Raja Abdullah, A. Ismail, and A. F. Abas, "A circular synthetic aperture radar for on-the-ground object detection," *Progress In Electromagnetics Research*, Vol. 122, 269–292, 2012.
10. Tian, B., D. Y. Zhu, and Z. D. Zhu, "A novel moving target detection approach for dual-channel SAR system," *Progress In Electromagnetics Research*, Vol. 115, 191–206, 2011.
11. Park, S. H., J. H. Lee, and K. T. Kim, "Performance analysis

of the scenario-based construction method for real target ISAR recognition progress," *Progress In Electromagnetics Research*, Vol. 128, 137–151, 2012.

12. Chang, Y. L., C. Y. Chiang, and K.-S. Chen, "SAR image simulation with application to target recognition," *Progress In Electromagnetics Research*, Vol. 119, 35–57, 2011.
13. Park, J. I. and K. T. Kim, "A comparative study on ISAR imaging algorithms for radar target identification," *Progress In Electromagnetics Research*, Vol. 108, 155–175, 2010.
14. Frery, A. C., H. J. Muller, C. D. Costa, C. D. C. F. Yanasse, and S. J. S. Sant' Anna, "A model for extremely heterogeneous clutter," *IEEE Transactions on Geoscience and Remote Sensing*, Vol. 35, No. 3, 648–659, 1997.
15. Gao, G., "Statistical modeling of SAR images: A survey," *Sensors*, Vol. 10, 775–795 2010.
16. Zhang, Y. D., L. N. Wu, and G. Wei, "A new classifier for polarimetric SAR images," *Progress In Electromagnetics Research*, Vol. 94, 83–104, 2009.
17. Oliver, C. J., *Understanding Synthetic Aperture Radar Images*, Artech House Boston, London, USA, UK, 1998.
18. Tison, C., J. M. Nicolas, F. Tupin, and H. Maître, "A new statistical model for Markovian classification of urban areas in high-resolution SAR images," *IEEE Transactions on Geoscience and Remote Sensing*, Vol. 42, No. 10, 2046–2057, 2004.
19. Gao, G., "A parzen-window-kernel-based CFAR algorithm for ship detection in SAR images," *IEEE Geoscience and Remote Sensing Letters*, Vol. 8, No. 3, 557–561, 2011.
20. Moser, G., J. Zerubia, and S. B. Serpico, "Dictionary-based stochastic expectation-maximization for SAR amplitude probability density function estimation," *IEEE Transactions on Geoscience and Remote Sensing*, Vol. 44, No. 1, 188–200, 2006.
21. Luo, M. and K. M. Huang, "Prediction of the electromagnetic field in metallic enclosures using artificial neural networks," *Progress In Electromagnetics Research*, Vol. 116, 171–184, 2011.
22. Castaldi, G., V. Galdi, and G. Gerini, "Evaluation of a neural network-based adaptive beamforming scheme with magnitude-only constraints," *Progress In Electromagnetics Research B*, Vol. 11, 1–14, 2009.
23. Li, X. and J. Gao, "Pad modeling by using artificial neural network," *Progress In Electromagnetics Research*, Vol. 74, 167–180, 2007.

24. Tan, C. P., J. Y. Koay, K. S. Lim, H. T. Ewe, and H. T. Chuah, "Classification of multi-temporal SAR images for rice crops using combined entropy decomposition and support vector machine technique," *Progress In Electromagnetics Research*, Vol. 71, 19–39, 2007.
25. McLachlan, G. J. and D. Peel, *Finite Mixture Models*, Wiely, New York, 2000.
26. Jin, Y. Q., "Polarimetric scattering modeling and information retrieval of SAR remote sensing — A review of FDU work," *Progress In Electromagnetics Research*, Vol. 104, 333–384, 2010.
27. Liu, D., Y. Du, G. Sun, W. Z. Yan, and B. I. Wu, "Analysis of InSAR sensitivity to forest structure based on radar scattering model," *Progress In Electromagnetics Research*, Vol. 84, 149–171, 2008.
28. Tan, C. P., J. Y. Koay, K. S. Lim, H. T. Ewe, and H. T. Chuah, "Classification of multi-temporal SAR images for rice crops using combined entropy decomposition and support vector machine technique," *Progress In Electromagnetics Research*, Vol. 71, 19–39, 2007.
29. Li, H. C., W. Hong, Y. R. Wu, and P. Z. Fan, "On the Empirical-statistical modeling of SAR images with generalized gamma distribution," *IEEE J. Sel. Top. Signal Process.,* Vol. 5, No. 3, 386–397, 2011.
30. Nicolas, J. M., "Introduction to second kind statistic: Application of log-moments and log-cumulants to SAR image law analysis," *Trait. Signal*, Vol. 19, No. 3, 139–167, 2002.
31. Liu, Z. L. and J. Yang, "Analysis of electromagnetic scattering with higher-order moment method and nurbs model," *Progress In Electromagnetics Research*, Vol. 96, 83–100, 2009.
32. Varmazyar, S. H , M. Naser-Moghadasi, and Z. Masouri, "A moment method simulation of electromagnetic scattering from conducting bodies," *Progress In Electromagnetics Research*, Vol. 81, 99–119, 2008.
33. Wang, S., X. Guan, D. W. Wang, X. Ma, and Y. Su, "Electromagnetic scattering by mixed conducting/dielectric objects using higher-order MoM," *Progress In Electromagnetics Research*, Vol. 66, 51–63, 2006.
34. Gradshteyn, S. I. and I. M. Ryzhik, *Table of Integrals, Series, and Products*, 7th Edition, Academic Press, San Diego, CA, 2007.